

# ReCoSplat: Autoregressive Feed-Forward Gaussian Splatting Using Render-and-Compare

Freeman Cheng<sup>1</sup>, Botao Ye<sup>2</sup>, Xueting Li<sup>3</sup>, Junqi You<sup>4</sup>, Fangneng Zhan<sup>5</sup>, and Ming-Hsuan Yang<sup>1</sup>

<sup>1</sup> University of California Merced

<sup>2</sup> ETH Zurich

<sup>3</sup> NVIDIA

<sup>4</sup> Shanghai Jiao Tong University

<sup>5</sup> Hong Kong University of Science and Technology

**Abstract.** Online novel view synthesis remains challenging, requiring robust scene reconstruction from sequential, often unposed, observations. We present **ReCoSplat**, an autoregressive feed-forward Gaussian Splatting model supporting posed or unposed inputs, with or without camera intrinsics. While assembling local Gaussians using camera poses scales better than canonical-space prediction, it creates a dilemma during training: using ground-truth poses ensures stability but causes a distribution mismatch when predicted poses are used at inference. To address this, we introduce a Render-and-Compare (ReCo) module. ReCo renders the current reconstruction from the predicted viewpoint and compares it with the incoming observation, providing a stable conditioning signal that compensates for pose errors. To support long sequences, we propose a hybrid KV cache compression strategy combining early-layer truncation with chunk-level selective retention, reducing the KV cache size by over 90% for 100+ frames. ReCoSplat achieves state-of-the-art performance across different input settings on both in- and out-of-distribution benchmarks. Code and pretrained models will be released. Our project page is at <https://freemancheng.com/ReCoSplat>.

**Keywords:** Novel view synthesis · Gaussian Splatting · feed-forward networks

## 1 Introduction

Novel view synthesis aims to render photorealistic images of a scene from unseen viewpoints. Among scene representations, 3D Gaussians have been widely adopted due to their high-quality real-time rendering. However, optimization-based Gaussian Splatting [12] requires lengthy per-scene training, limiting real-time applications. Feed-forward Gaussian Splatting [1, 10, 23, 32, 35, 36, 40] predicts 3D Gaussians directly from input images, bypassing per-scene optimization. Yet these approaches target offline reconstruction, where all images are available upfront. The autoregressive setting, where observations arrive sequentially, remains largely unexplored despite its importance for embodied AI, AR/VR, and



**Fig. 1: Autoregressive Reconstruction.** We present ReCoSplat, a method that reconstructs 3D scenes from sequential image streams.

video generation [2, 30]. This motivates feed-forward methods capable of synthesizing novel views in real time as observations arrive.

We present ReCoSplat, an autoregressive feed-forward Gaussian Splatting method for scene reconstruction from hundreds of images in posed or unposed settings, with or without camera intrinsics. In practice, camera parameters vary widely: extrinsics may come from sensors or be missing, while intrinsics may exist in metadata or be removed. A robust method must handle these diverse combinations of sensor inputs.

Recent work demonstrates that predicting Gaussians in local camera space and mapping them to world coordinates via camera poses, which we term **assembly poses**, yields better scalability than predicting directly in a canonical space [35, 36]. However, a critical design choice is whether to use ground-truth or predicted assembly poses during training, a decision that divides existing autoregressive methods. StreamGS [13] and SaLon3R [8] use predicted poses, but this couples Gaussian prediction with pose estimation and leads to instability [35]. Using ground-truth poses decouples the tasks, as in LongSplat [9], but assumes camera poses are provided. A natural alternative is to train with ground-truth poses and switch to predicted poses at inference. However, this introduces a **pose distribution mismatch**, causing misaligned Gaussians. While offline models such as YoNoSplat [35] mitigate this with training curricula, we find such strategies ineffective in the autoregressive setting where pose estimation is more challenging.

To address pose distribution mismatch from training with ground-truth assembly poses, ReCoSplat introduces a **Render-and-Compare** module inspired by the Analysis-by-Synthesis framework [38]. This paradigm treats vision as an inverse problem, where predictions are refined by comparing synthesized views with observations. Accordingly, when predicting Gaussians for a new observa-

tion, our module renders the current reconstruction from the assembly pose and compares it with the incoming image. The rendered–observed pair captures pose discrepancies and provides a stable geometric and visual prior that guides Gaussian prediction via cross-attention. To enrich this signal, we augment each Gaussian with additional feature dimensions beyond RGB.

To scale ReCoSplat to hundreds of frames, we address the KV-cache memory bottleneck in transformer backbones such as  $\pi^3$  [27]. Since early global attention layers contribute little to multi-view correspondence [21], we discard KV caches for the first 10 of  $\pi^3$ 's 18 layers. In the remaining 8 layers, we retain tokens only from every  $n$ -th view. To avoid information loss, we process frames in chunks of size  $n$ , where all views attend within the chunk before non-retained tokens are dropped. To establish a comprehensive initial context, the first chunk is processed without any pruning, and a trainable register token is introduced to explicitly mark the retained views. We employ curriculum learning with variable chunk sizes (4–8) during training, ensuring that  $n$  remains dynamically configurable at test time. Ultimately, with a chunk size of 8, our strategy successfully prunes over 90% of KV-cache tokens for sequences containing 100 or more images.

The contributions of this work are:

- **Render-and-Compare module.** We render the accumulated scene onto each incoming view and use the rendered–observed comparison as a conditioning signal, bridging the pose distribution mismatch between ground-truth and predicted assembly poses.
- **KV cache compression.** We combine early-layer truncation with selective single-view retention guided by a learned prompt register token, reducing KV cache memory by 10× for 100-image sequences and enabling real-time reconstruction on consumer hardware.
- **State-of-the-art results.** We evaluate across diverse input settings (posed or unposed, with or without intrinsics), on both in- and out-of-distribution datasets and diverse camera trajectories, achieving consistent state-of-the-art performance.

## 2 Related Work

**Feed-Forward Multi-View Stereo.** Feed-forward Multi-View Stereo (MVS) methods predict dense geometry directly from RGB images. Early methods such as MVNet [33, 34] construct cost volumes but require known camera parameters. DUST3R [26] removes this constraint by predicting 3D pointmaps from image pairs in the first-view camera space. Later methods extend to multi-view settings using alternating attention [11, 24], while  $\pi^3$  [27] shows that canonical first-view coordinates introduce harmful inductive bias. Depth Anything 3 [15] demonstrates that standard transformers without specialized alternating attention can better exploit pretrained weights. Several methods further extend MVS to streaming settings. WinT3R [14] maintains a sliding window and accumulates camera tokens. Point3R [31] anchors history tokens to 3D positions via

spatial pointer memory. StreamVGGT [43] accumulates KV-cache with knowledge distillation. CUT3R [25] employs recurrent state memory updated with new observations. TTT3R [3] formulates the problem as test-time training [22] with confidence-guided learning rates for better length generalization. While these pointmap methods excel at geometry reconstruction, they lack rendering capabilities for real-time novel view synthesis, motivating our feed-forward autoregressive Gaussian Splatting.

**Feed-Forward Gaussian Splatting.** Feed-forward Gaussian Splatting predicts 3D Gaussian primitives directly from images, eliminating per-scene optimization [39]. Early methods [1, 23, 40] demonstrated novel view synthesis by predicting per-pixel Gaussians. Subsequent methods [10, 35, 36] leverage pre-trained models to improve geometry and reconstruction quality. Recent work extends this paradigm to autoregressive settings. StreamGS [13] processes unposed streams via cross-frame feature matching and adaptive density control. SaLon3R [8] compresses Gaussians into saliency-aware anchors refined by a point transformer. LongSplat [9] processes the current frame with temporal neighbors using DepthSplat [32] and encodes historical context through a Gaussian-Image Representation (GIR).

Our approach differs in several aspects. First, LongSplat requires ground-truth poses for Gaussian assembly. Second, it uses the GIR to encode historical context, whereas our Render-and-Compare module improves generalization from ground-truth to predicted assembly poses. Third, using the GIR within our ReCo module degrades performance. Although not designed for streaming, FreeSplat [28] can be adapted to causal processing by restricting fusion to past frames. FreeSplat aligns local and global Gaussians based on depth proximity and merges them via a GRU. As existing streaming methods lack public code, we adopt FreeSplat as a baseline.

## 3 Method

An overview of ReCoSplat is shown in Figure 2.

### 3.1 Problem Formulation

ReCoSplat reconstructs a 3D scene from a continuous image stream processed in non-overlapping chunks of  $n \in [4, 8]$  images. At timestep  $t$ , the autoregressive network  $f_\theta$  receives a new image chunk  $\mathbf{I}_t = (I_t^1, \dots, I_t^n)$ , optional camera parameters  $\mathbf{K}_t = (K_t^1, \dots, K_t^n)$  (intrinsics) and  $\mathbf{P}_t = (P_t^1, \dots, P_t^n)$  (extrinsics), the KV cache  $M_{t-1}$  from previous chunks, and the accumulated scene  $S_{t-1}$  containing all previously predicted 3D Gaussians. The model estimates:

$$(\mathbf{G}_t, \hat{\mathbf{K}}_t, \hat{\mathbf{P}}_t, M_t) = f_\theta(\mathbf{I}_t, \mathbf{K}_t, \mathbf{P}_t, M_{t-1}, S_{t-1}), \quad (1)$$

where  $\mathbf{G}_t = (G_t^1, \dots, G_t^n)$  are the predicted local Gaussians,  $\hat{\mathbf{K}}_t$  and  $\hat{\mathbf{P}}_t$  are the predicted intrinsic and extrinsic camera parameters, and  $M_t$  is the updated

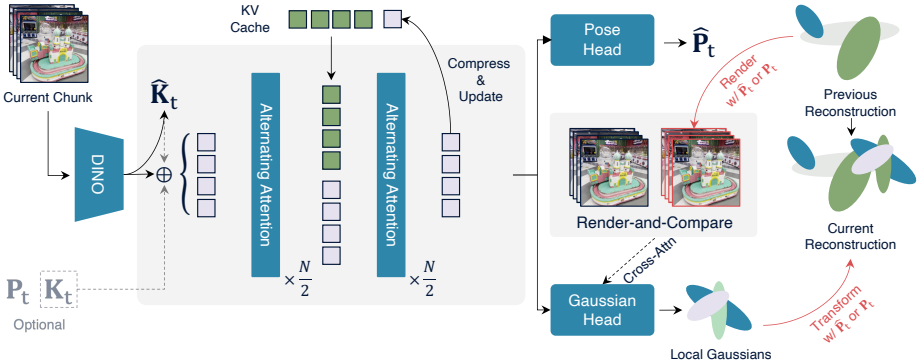


**Fig. 2: ReCoSplat overview.** Given a chunk of input images, a DINO-based encoder extracts features, which are then processed by an alternating-attention transformer with an autoregressive KV cache. The pose head predicts camera poses, while the Gaussian head predicts local Gaussian primitives. To bridge the pose distribution mismatch between training and inference, the Render-and-Compare module renders the current reconstruction at the assembly pose and compares it with the incoming observation to provide conditioning via cross-attention. The predicted local Gaussians are then transformed to world coordinates and merged into the accumulated scene.

KV cache. Each set of local Gaussians  $G_t^k$  is defined in the camera space of image  $I_t^k$ . To merge  $G_t^k$  into the accumulated scene  $S_{t-1}$ , we transform it into world coordinates using either ground-truth or predicted camera poses depending on the input setting. We define this pose as the **assembly pose**  $A_t^k$ . Using  $\mathbf{A}_t = (A_t^1, \dots, A_t^n)$ , we update the scene by merging the local Gaussians:

$$S_t = S_{t-1} \cup \text{Transform}(\mathbf{G}_t, \mathbf{A}_t). \quad (2)$$

### 3.2 Autoregressive Backbone

ReCoSplat processes images with an autoregressive backbone based on YoNoSplat [35], augmented with a KV cache.

**Encoder and Decoder.** Given an image chunk  $\mathbf{I}_t$ , a ViT encoder [6] initialized with DINOv2 [18] maps each image  $I_t^k$  to a global camera token  $c_t^k$  and patch tokens  $E_t^k$ :

$$[c_t^k, E_t^k] = \text{Encoder}(I_t^k) \quad (3)$$

Camera intrinsics are predicted from the camera token via a two-layer MLP:  $\hat{K}_t^k = \text{Head}_{\text{intrinsics}}(c_t^k)$ . The patch tokens  $\mathbf{E}_t = (E_t^1, \dots, E_t^n)$  are processed by a 36-layer alternating-attention transformer decoder [27], interleaving frame and global attention, to produce multi-view features  $\mathbf{F}_t = (F_t^1, \dots, F_t^n)$ .

**Prediction Heads.** The prediction heads include a pose head and three Gaussian heads that decode each Gaussian’s position, attributes, and features. The pose head predicts camera extrinsics from decoder features:  $\hat{P}_t^k = \text{Head}_{\text{extrinsics}}(F_t^k)$ .

The Gaussian heads predict primitives from  $2\times$  upsampled features  $(F_t^k)^{2\times}$ , each conditioned on tokens  $Z_t^k$  from the Render-and-Compare module (Section 3.3) via cross-attention:

$$G_t^k = \left[ \text{Head}_{\text{xyz}}((F_t^k)^{2\times}, Z_t^k), \text{Head}_{\text{gs}}((F_t^k)^{2\times}, Z_t^k), \text{Head}_{\text{feat}}((F_t^k)^{2\times}, Z_t^k) \right]. \quad (4)$$

The pose head uses a five-layer frame-wise transformer followed by a two-layer MLP. The position and attribute heads each use a five-layer transformer with a linear projection. The feature head is a DPT [19] that takes  $(F_t^k)^{2\times}$  and intermediate activations from the position head as input, which performs better than an identical branch.

**KV Cache.** To enable autoregressive processing, we maintain a KV cache for the last 8 global attention layers of the transformer decoder. At timestep  $t$ , the decoder processes current patch tokens  $\mathbf{E}_t$  together with cached keys and values  $M_{t-1}$  from previous chunks. In global attention layers, each patch token attends to tokens in the current chunk and those stored in  $M_{t-1}$ . The KV cache is updated after each timestep:

$$\mathbf{F}_t, M_t = \text{Decoder}(\mathbf{E}_t, M_{t-1}). \quad (5)$$

### 3.3 Render-and-Compare Module

Existing methods use either predicted [8] or ground-truth [9] poses for local Gaussian assembly. The former couples Gaussian prediction with pose estimation, limiting reconstruction quality while the latter biases predictions toward ground-truth poses, creating a pose distribution mismatch when predicted poses are used at inference (Sections 4.2, 4.3). An intuitive alternative is a curriculum mixing both pose sources [35]. However, this strategy is ineffective because pose estimation is more difficult in the autoregressive setting, so predicted assembly poses are noisy and provide weak supervision (Section 4.3).

To address pose distribution mismatch, we introduce a Render-and-Compare module that enables generalization from training with ground-truth to inference with predicted assembly poses. For each image  $I_t^k$  in the current chunk, we render the accumulated scene  $S_{t-1}$  at its assembly pose  $A_t^k$ :

$$\hat{R}_t^k = \text{Render}(S_{t-1}, A_t^k) \quad (6)$$

where  $\hat{R}_t^k \in \mathbb{R}^{H \times W \times 12}$  contains RGB and 9 learned feature channels decoded by a feature head (Section 3.2). When ground-truth intrinsics are unavailable, we use our predicted intrinsics for rendering to prevent information leakage. Afterwards, we concatenate the rendering with the input image and obtain conditioning tokens:

$$Z_k = \text{Patchify}([I_k, \hat{R}_k]). \quad (7)$$

Patchify maps the concatenation to token space using three convolutional layers with strided downsampling. These tokens guide Gaussian prediction via cross-attention (Section 3.2). Since changes in  $A_t^k$  directly affect the rendered image  $\hat{R}_t^k$ , this module improves generalization to predicted poses at inference (Table 1).

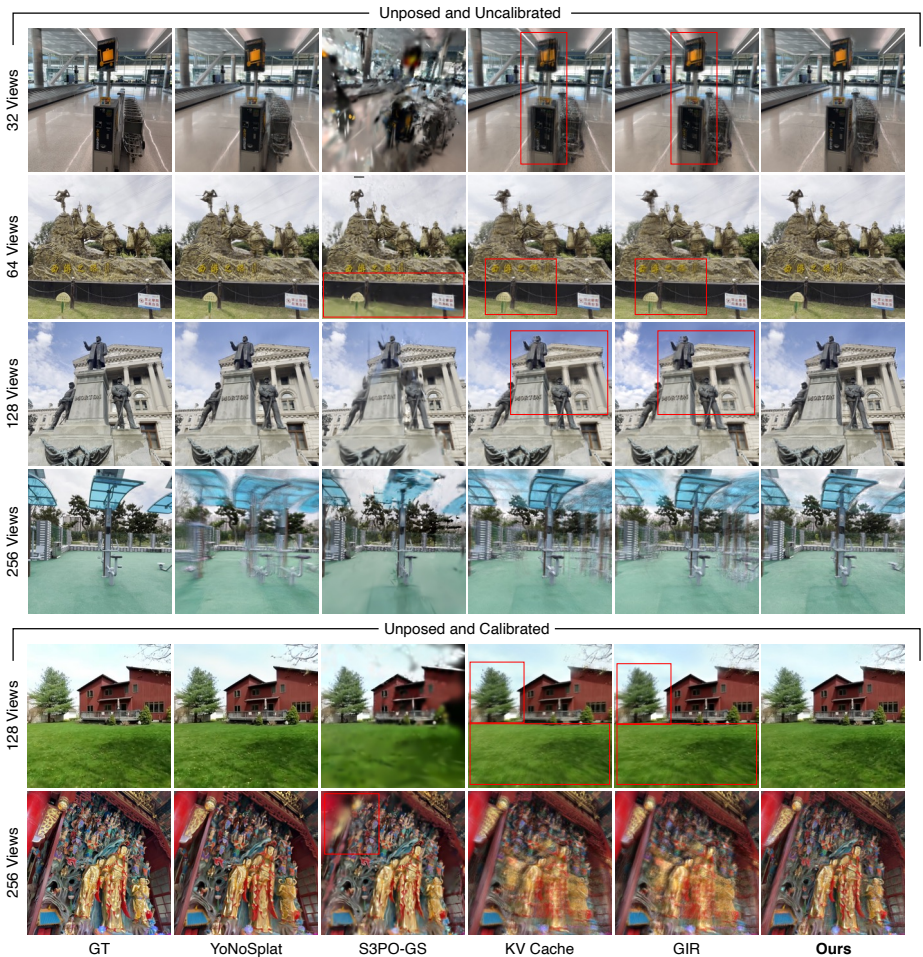


**Fig. 3:** Novel view synthesis with increasing input views under unposed settings. ReCoSplat improves geometry and reduces artifacts over autoregressive baselines.

### 3.4 Efficient Long-Sequence Reconstruction

Scaling ReCoSplat to process hundreds of images is fundamentally constrained by the memory demands of its transformer architecture. Continuously accumulating the KV cache for every image across all global attention layers causes VRAM usage to grow rapidly with sequence length, rendering long-sequence inference impractical on consumer hardware. To overcome this bottleneck, we introduce two complementary KV cache compression strategies.

**Early Layer Truncation.** We introduce a KV cache truncation mechanism based on the finding that early global attention layers extract local features rather than establishing multi-view correspondences [21]. By omitting the KV

cache for the first 10 of the 18 global attention layers, we restrict attention in these layers to the current chunk, significantly reducing memory overhead without sacrificing global context.

**Selective Context Retention.** For the remaining 8 global attention layers, entirely discarding historical tokens would severely degrade reconstruction quality. Instead, we compress the context using a chunk-wise retention strategy. To establish a robust initial context, the first chunk (size 8) retains KV tokens for all its images. For subsequent chunks of size  $n \in [4, 8]$ , we retain tokens from only a single representative view—the final frame of the chunk. To ensure the network effectively utilizes this compressed cache, we assign a distinct, trainable register token to these retained views.

**Memory Complexity Analysis.** This two-stage strategy changes the memory scaling of the network. A standard multi-view transformer stores per-image KV tokens across all  $L = 18$  layers for  $N$  images, yielding space complexity  $\Theta(L \cdot N)$ . Our method stores no historical tokens for the first 10 layers. For the remaining 8 layers, we keep tokens for the initial 8-image chunk and one set for each of the  $\frac{N-8}{n}$  subsequent chunks, totaling  $8(8 + \frac{N-8}{n})$  token sets. The asymptotic space complexity thus becomes  $\Theta(\frac{N}{n})$ , significantly reducing the constant factor. For  $N = 256$  and  $n = 8$ , a standard cache stores 4608 token sets, while our method stores only 312, reducing memory by 93% and enabling efficient autoregressive rendering on consumer hardware. The effect of our KV cache compression strategies on the overall VRAM usage of our model is depicted in Figure 5.

### 3.5 Training and Inference

**Stages.** Training proceeds in three stages, each building on the previous to progressively introduce the capabilities of ReCoSplat. In **Stage 1**, we initialize from YoNoSplat’s [35] DL3DV-10K [16] checkpoint and train for 150k steps with learning rate  $5 \times 10^{-6}$ , keeping the encoder frozen. We sample 2–64 context views per iteration, linearly increasing the maximum from 8 to 64 between steps 1.5k and 75k. The chunk size is fixed at 8 and no KV cache compression is applied. In **Stage 2**, we train for 50k additional steps at  $5 \times 10^{-7}$  and introduce variable chunk sizes after the first chunk, sampling uniformly from [4, 8] while annealing the minimum from 8 to 4 over the first 25k steps. The first chunk remains fixed at 8 to anchor the scene representation. In **Stage 3**, we train for a final 50k steps at the same learning rate and enable the full KV cache compression strategy (Section 3.4). All stages use 8 GPUs with batch size 1.

**Losses.** ReCoSplat is supervised with a multi-task loss that balances photometric quality, camera estimation accuracy, and Gaussian sparsity:

$$\mathcal{L} = \mathcal{L}_{\text{MSE}} + \mathcal{L}_{\text{LPIPS}} + \mathcal{L}_{\text{intrinsic}} + \mathcal{L}_{\text{extrinsic}} + \mathcal{L}_{\text{opacity}}. \quad (8)$$

The photometric term combines pixel-wise MSE ( $\mathcal{L}_{\text{MSE}}$ ) and perceptual similarity ( $\mathcal{L}_{\text{LPIPS}}$ ) [41], computed between eight novel target views rendered from the predicted Gaussians and held-out ground-truth images. Camera supervision is decomposed into intrinsic and extrinsic terms:  $\mathcal{L}_{\text{intrinsic}}$  penalizes the  $\ell_2$  error

between predicted and ground-truth focal lengths, while  $\mathcal{L}_{\text{extrinsic}}$  applies a pairwise relative pose loss over all inputs. To encourage sparsity,  $\mathcal{L}_{\text{opacity}}$  imposes an  $\ell_1$  penalty on Gaussian opacities, and Gaussians with opacity below 0.005 are pruned. We set loss weights to  $\lambda_{\text{MSE}} = 1.0$ ,  $\lambda_{\text{LPIPS}} = 0.05$ ,  $\lambda_{\text{intrinsic}} = 0.5$ ,  $\lambda_{\text{extrinsic}} = 0.1$ , and  $\lambda_{\text{opacity}} = 0.01$ . Complete formulations are provided in the appendix.

**Scale Alignment.** During inference, ReCoSplat accepts either ground-truth or predicted camera poses as the assembly poses. When ground-truth extrinsics are available, they are not required to be metric. Instead, we align their scale to be consistent with the model’s predicted poses before assembling local Gaussians. Specifically, we compute a fixed global scaling factor by matching the scale of the first chunk’s ground-truth poses  $\mathbf{P}_1$  to that of the first chunk’s predicted poses  $\hat{\mathbf{P}}_1$ , where  $\text{Scale}(\cdot)$  denotes the maximum pairwise camera translation within a set of poses. Formally, the assembly pose

$$A_t^k = \begin{cases} \frac{\text{Scale}(\mathbf{P}_1)}{\text{Scale}(\hat{\mathbf{P}}_1)} P_t^k & \text{if GT extrinsics are available,} \\ \hat{P}_t^k & \text{otherwise.} \end{cases} \quad (9)$$

It is necessary to use the first chunk for scale alignment. Unlike offline methods that can normalize over the full trajectory [35], an autoregressive model has no access to future poses and must commit to a scale at the very first chunk.

## 4 Experiments

### 4.1 Experimental Setup

**Datasets.** We train and evaluate ReCoSplat on DL3DV [16] (9,894 train / 140 test) and ScanNet++ (968 train / 50 test) [37], sampled at a 10:1 ratio during training. DL3DV contains diverse indoor and outdoor scenes, while ScanNet++ focuses on room-scale indoor scenes with more irregular camera trajectories. To assess generalization, we also evaluate on RealEstate10K (indoor/outdoor real estate videos) [42], ACID (aerial coastline videos) [17], and ScanNet (room-scale indoor captures) [5]. Due to large scene-size variance, we restrict RealEstate10K and ACID to scenes with at least 200 images (1648 for RealEstate10K, 755 for ACID). For ScanNet, we evaluate on 8 scenes following [29] for fair comparison. Context views are selected via farthest point sampling on ground-truth camera positions. For each scene, 8 target novel views are held out by dividing remaining frames into 8 bins and sampling one image from each bin.

**Evaluated Methods.** We compare ReCoSplat with YoNoSplat [35], FreeSplat [29], and S3PO-GS [4] for novel view synthesis. Recent autoregressive feed-forward methods (StreamGS [13], SaLon3R [8], LongSplat [9]) are excluded due to unavailable code. YoNoSplat serves as an offline feed-forward baseline and is fine-tuned on our dataset split and training setup for fair comparison. FreeSplat is an offline method that can be adapted to autoregressive inference by restricting cost volumes to past frames; we instead evaluate the original model as an



**Fig. 4:** Novel view synthesis in the fully posed and calibrated setting with 128 and 256 input views. With pose errors removed, reconstruction quality depends on local Gaussian prediction accuracy. Our method module can correct for local Gaussian mispredictions, outperforming autoregressive baselines and beating YoNoSplat in PSNR.

upper bound. Since FreeSplat is trained on only 100 ScanNet scenes, we evaluate it only on ScanNet. S3PO-GS represents optimization-based autoregressive methods but is excluded from RealEstate10K due to costly per-scene optimization.

To approximate a comparison with LongSplat without access to its codebase, we train a version of ReCoSplat using LongSplat’s Gaussian Image Representation (GIR) as the cross-attention conditioning signal, denoted **GIR**. We also include an ablation removing the Render-and-Compare module, denoted **KV Cache**. For camera pose estimation, we compare with YoNoSplat and representative online methods with different memory designs: CUT3R and TTT3R (recurrent state) [3, 25], StreamVGGT (uncompressed KV cache) [43], and WinT3R (growing camera token pool) [14].

**Metrics.** We evaluate novel view synthesis using PSNR, SSIM, and LPIPS. In the posed setting, targets are rendered at ground-truth poses. In the unposed setting, we follow prior pose-free works [7, 20] and predict target poses for rendering. Specifically, target poses are predicted through 100 iterations of pose optimization using the rendering loss. For camera pose estimation, we report the area under the cumulative angular pose error curve (AUC) at  $5^\circ$ ,  $10^\circ$ , and  $15^\circ$  thresholds.

**Implementation Details.** We train ReCoSplat at  $224 \times 224$  resolution using A6000 48GB GPUs. Ablations and baseline fine-tuning use A6000 48GB, A100 40GB, or H100 80GB GPUs depending on availability. All experiments use 8 GPUs with batch size 1. Some baselines operate at higher resolutions; in such cases, we ensure our inputs cover a smaller receptive field for fair comparison. For evaluation, rendered outputs are center-cropped and rescaled to  $224 \times 224$ .

**Table 1:** Novel view synthesis on DL3DV with 32, 64, 128, and 256 input views sampled from the first 180, 240, 300, and (up to) 360 frames of each scene, respectively. **Best** and **second best** metrics are marked, excluding offline methods.

| Method    | Online $p$ | $k$          | 32v             |                 |                    | 64v             |                 |                    | 128v            |                 |                    | 256v            |                 |                    |
|-----------|------------|--------------|-----------------|-----------------|--------------------|-----------------|-----------------|--------------------|-----------------|-----------------|--------------------|-----------------|-----------------|--------------------|
|           |            |              | PSNR $\uparrow$ | SSIM $\uparrow$ | LPIPS $\downarrow$ | PSNR $\uparrow$ | SSIM $\uparrow$ | LPIPS $\downarrow$ | PSNR $\uparrow$ | SSIM $\uparrow$ | LPIPS $\downarrow$ | PSNR $\uparrow$ | SSIM $\uparrow$ | LPIPS $\downarrow$ |
| YoNoSplat | $\times$   |              | 22.368          | 0.736           | 0.180              | 22.253          | 0.732           | 0.183              | 21.827          | 0.720           | 0.194              | 20.749          | 0.677           | 0.226              |
| KV Cache  |            |              | 21.705          | <b>0.703</b>    | <b>0.202</b>       | 21.302          | 0.680           | 0.223              | 20.784          | 0.655           | 0.247              | 19.819          | 0.606           | 0.292              |
| GIR       |            |              | <b>21.752</b>   | <b>0.703</b>    | 0.203              | <b>21.382</b>   | <b>0.682</b>    | <b>0.222</b>       | <b>20.933</b>   | <b>0.660</b>    | <b>0.245</b>       | <b>19.900</b>   | <b>0.608</b>    | <b>0.291</b>       |
| Ours      |            |              | <b>22.097</b>   | <b>0.716</b>    | <b>0.194</b>       | <b>21.774</b>   | <b>0.696</b>    | <b>0.213</b>       | <b>21.284</b>   | <b>0.672</b>    | <b>0.235</b>       | <b>20.220</b>   | <b>0.617</b>    | <b>0.281</b>       |
| YoNoSplat | $\times$   | $\checkmark$ | 22.575          | 0.748           | 0.177              | 22.514          | 0.747           | 0.179              | 22.053          | 0.735           | 0.189              | 20.953          | 0.692           | 0.221              |
| S3PO-GS   |            | $\checkmark$ | 13.062          | 0.197           | 0.635              | 13.952          | 0.217           | 0.645              | 17.227          | 0.375           | 0.548              | 13.102          | 0.196           | 0.697              |
| KV Cache  |            | $\checkmark$ | 21.932          | <b>0.717</b>    | <b>0.198</b>       | 21.544          | <b>0.697</b>    | <b>0.218</b>       | 20.993          | 0.670           | 0.242              | 20.007          | <b>0.622</b>    | <b>0.286</b>       |
| GIR       |            | $\checkmark$ | <b>21.947</b>   | 0.716           | 0.199              | <b>21.600</b>   | <b>0.697</b>    | <b>0.218</b>       | <b>21.107</b>   | <b>0.672</b>    | <b>0.241</b>       | <b>20.085</b>   | <b>0.622</b>    | <b>0.286</b>       |
| Ours      |            | $\checkmark$ | <b>22.417</b>   | <b>0.734</b>    | <b>0.188</b>       | <b>22.068</b>   | <b>0.713</b>    | <b>0.206</b>       | <b>21.576</b>   | <b>0.690</b>    | <b>0.227</b>       | <b>20.430</b>   | <b>0.633</b>    | <b>0.275</b>       |
| YoNoSplat | $\times$   | $\checkmark$ | 22.998          | 0.781           | 0.162              | 22.978          | 0.784           | 0.161              | 22.597          | 0.779           | 0.167              | 21.549          | 0.749           | 0.190              |
| KV Cache  |            | $\checkmark$ | 22.392          | 0.758           | <b>0.177</b>       | 22.210          | 0.754           | <b>0.184</b>       | 21.731          | <b>0.739</b>    | <b>0.199</b>       | 20.694          | <b>0.699</b>    | <b>0.235</b>       |
| GIR       |            | $\checkmark$ | <b>22.478</b>   | <b>0.760</b>    | <b>0.177</b>       | <b>22.264</b>   | <b>0.755</b>    | 0.185              | <b>21.779</b>   | <b>0.739</b>    | 0.200              | <b>20.743</b>   | <b>0.699</b>    | <b>0.235</b>       |
| Ours      |            | $\checkmark$ | <b>23.084</b>   | <b>0.780</b>    | <b>0.164</b>       | <b>23.086</b>   | <b>0.782</b>    | <b>0.167</b>       | <b>22.852</b>   | <b>0.777</b>    | <b>0.176</b>       | <b>22.003</b>   | <b>0.751</b>    | <b>0.202</b>       |

## 4.2 Experiment Results

**Novel View Synthesis.** We evaluate ReCoSplat on novel view synthesis across three input settings: uncalibrated and unposed, unposed, and fully posed and calibrated. To comprehensively assess our method, we consider multiple datasets with varying sequence lengths, scene scales, and camera trajectories. On DL3DV, we evaluate using 32 to 256 input views where the scene scale increases with the number of views (Table 1), and separately with 90 to 270 views sampled from the entire sequence (Table 2). To test robustness under challenging unsmooth camera motion that is unfriendly to the online reconstruction task, we further evaluate on ScanNet++ with up to 512 input views (Table 3). Across all settings, ReCoSplat consistently outperforms autoregressive baselines. **In particular, the substantial improvements in unposed settings demonstrate that our method effectively adapts to predicted assembly poses at inference time.** Qualitatively, these improvements are reflected in Figure 3, where ReCoSplat produces sharper geometry and fewer artifacts than competing online methods. Note that although S3PO-GS needs calibrated inputs, we also compare against it in the uncalibrated setting here. While our metrics trail the offline baseline, YoNoSplat, which has access to the entire image sequence upfront, ReCoSplat delivers highly competitive performance under the strictly harder constraints of autoregressive reconstruction. In the unposed setting, online methods encounter three coupled error sources: pose distribution mismatch, local Gaussian prediction error, and pose estimation error. **A major advantage of our proposed Render-and-Compare module is that it directly tackles the first two error sources.** The effectiveness of the ReCo module is further evident in the fully posed and calibrated setting. When there is no pose prediction error, ReCoSplat approaches YoNoSplat’s performance and even surpasses it in PSNR (Table 1, Figure 4). This result provides strong evidence that as camera pose estimation improves, ReCoSplat’s performance in unposed settings should improve correspondingly. Interestingly, using ground-truth poses

**Table 2:** Novel view synthesis on ScanNet (out-of-distribution) and DL3DV. Following FreeSplat’s average frame interval of 20, ScanNet inputs are from the first 640 frames, while DL3DV uses the entire sequence. **Best** and **second best** metrics are marked.

| Method    | $p$ | $k$ | ScanNet         |                 |                    |                 |                 |                    | DL3DV           |                 |                    |                 |                 |                    |
|-----------|-----|-----|-----------------|-----------------|--------------------|-----------------|-----------------|--------------------|-----------------|-----------------|--------------------|-----------------|-----------------|--------------------|
|           |     |     | 32v             |                 |                    | 90v             |                 |                    | 180v            |                 |                    | 270v            |                 |                    |
|           |     |     | PSNR $\uparrow$ | SSIM $\uparrow$ | LPIPS $\downarrow$ | PSNR $\uparrow$ | SSIM $\uparrow$ | LPIPS $\downarrow$ | PSNR $\uparrow$ | SSIM $\uparrow$ | LPIPS $\downarrow$ | PSNR $\uparrow$ | SSIM $\uparrow$ | LPIPS $\downarrow$ |
| S3PO-GS   | ✓   |     | 12.820          | 0.511           | 0.640              | 12.482          | 0.169           | 0.728              | 14.976          | 0.255           | 0.658              | 12.471          | 0.177           | 0.708              |
| KV Cache  | ✓   |     | 25.384          | <b>0.828</b>    | <b>0.207</b>       | 20.703          | 0.654           | 0.248              | 20.318          | 0.635           | 0.269              | 19.922          | <b>0.614</b>    | <b>0.293</b>       |
| GIR       | ✓   |     | <b>25.426</b>   | 0.826           | 0.211              | <b>20.886</b>   | <b>0.662</b>    | <b>0.244</b>       | <b>20.461</b>   | <b>0.640</b>    | <b>0.268</b>       | <b>19.949</b>   | 0.613           | 0.294              |
| Ours      | ✓   |     | <b>25.830</b>   | <b>0.830</b>    | <b>0.205</b>       | <b>21.206</b>   | <b>0.670</b>    | <b>0.237</b>       | <b>20.823</b>   | <b>0.651</b>    | <b>0.259</b>       | <b>20.325</b>   | <b>0.625</b>    | <b>0.282</b>       |
| FreeSplat | ✓   | ✓   | 22.691          | 0.730           | 0.255              | N/A             | N/A             | N/A                | N/A             | N/A             | N/A                | N/A             | N/A             | N/A                |
| KV Cache  | ✓   | ✓   | 23.252          | 0.761           | <b>0.245</b>       | 21.478          | 0.729           | <b>0.206</b>       | 21.104          | 0.716           | <b>0.219</b>       | 20.558          | <b>0.694</b>    | <b>0.240</b>       |
| GIR       | ✓   | ✓   | <b>23.315</b>   | <b>0.763</b>    | 0.246              | <b>21.556</b>   | <b>0.730</b>    | <b>0.206</b>       | <b>21.166</b>   | <b>0.717</b>    | <b>0.219</b>       | <b>20.598</b>   | <b>0.694</b>    | 0.241              |
| Ours      | ✓   | ✓   | <b>24.073</b>   | <b>0.789</b>    | <b>0.223</b>       | <b>22.408</b>   | <b>0.758</b>    | <b>0.188</b>       | <b>22.280</b>   | <b>0.759</b>    | <b>0.193</b>       | <b>21.866</b>   | <b>0.748</b>    | <b>0.206</b>       |

**Table 3:** Novel view synthesis on RealEstate10K (out-of-distribution) and ScanNet++. Input views are sampled from the entire test sequence. For ScanNet++, we evaluate on 46/50 scenes for 256 views and 30/50 scenes for 512 views due to limited sequence length. The **best** and **second best** metrics are marked.

| Method   | $p$ | $k$ | RealEstate10K   |                 |                    |                 |                 |                    | ScanNet++       |                 |                    |                 |                 |                    |
|----------|-----|-----|-----------------|-----------------|--------------------|-----------------|-----------------|--------------------|-----------------|-----------------|--------------------|-----------------|-----------------|--------------------|
|          |     |     | 64v             |                 |                    | 128v            |                 |                    | 256v            |                 |                    | 512v            |                 |                    |
|          |     |     | PSNR $\uparrow$ | SSIM $\uparrow$ | LPIPS $\downarrow$ | PSNR $\uparrow$ | SSIM $\uparrow$ | LPIPS $\downarrow$ | PSNR $\uparrow$ | SSIM $\uparrow$ | LPIPS $\downarrow$ | PSNR $\uparrow$ | SSIM $\uparrow$ | LPIPS $\downarrow$ |
| S3PO-GS  | ✓   |     | N/A             | N/A             | N/A                | N/A             | N/A             | N/A                | 8.668           | 0.156           | 0.759              | 11.547          | 0.337           | 0.752              |
| KV Cache | ✓   |     | <b>24.860</b>   | <b>0.858</b>    | <b>0.138</b>       | <b>23.640</b>   | <b>0.820</b>    | 0.175              | 18.917          | 0.652           | 0.355              | 18.155          | <b>0.625</b>    | <b>0.405</b>       |
| GIR      | ✓   |     | 24.787          | 0.856           | 0.140              | 23.629          | <b>0.820</b>    | <b>0.173</b>       | <b>19.072</b>   | <b>0.657</b>    | <b>0.353</b>       | <b>18.247</b>   | <b>0.632</b>    | <b>0.403</b>       |
| Ours     | ✓   |     | <b>25.705</b>   | <b>0.873</b>    | <b>0.128</b>       | <b>24.713</b>   | <b>0.844</b>    | <b>0.155</b>       | <b>19.660</b>   | <b>0.663</b>    | <b>0.342</b>       | <b>18.289</b>   | 0.611           | 0.411              |
| KV Cache | ✓   | ✓   | <b>24.490</b>   | <b>0.856</b>    | <b>0.138</b>       | 23.179          | 0.819           | 0.175              | 19.287          | <b>0.700</b>    | <b>0.305</b>       | 18.466          | 0.680           | 0.346              |
| GIR      | ✓   | ✓   | 24.423          | 0.854           | 0.140              | <b>23.255</b>   | <b>0.822</b>    | <b>0.171</b>       | <b>19.331</b>   | 0.699           | 0.308              | <b>18.514</b>   | <b>0.682</b>    | <b>0.343</b>       |
| Ours     | ✓   | ✓   | <b>25.830</b>   | <b>0.884</b>    | <b>0.120</b>       | <b>24.957</b>   | <b>0.864</b>    | <b>0.143</b>       | <b>20.797</b>   | <b>0.746</b>    | <b>0.263</b>       | <b>20.308</b>   | <b>0.734</b>    | <b>0.287</b>       |

unexpectedly degrades performance in our ScanNet evaluations (Table 2). We attribute this to inaccuracies in ScanNet’s ground-truth camera poses, which introduce assembly errors when used directly.

**Camera Pose Estimation.** Table 4 reports camera pose estimation performance measured by AUC of the angular pose error curve at  $5^\circ$ ,  $10^\circ$ , and  $20^\circ$  thresholds on ACID, RealEstate10K, and DL3DV. We compare ReCoSplat with several representative online reconstruction methods employing different memory designs, including recurrent state models (CUT3R, TTT3R), persistent token memories (WinT3R), and uncompressed KV-cache architectures (StreamVGGT). The compared methods are trained on different datasets. Both ReCoSplat and YoNoSplat are trained only on DL3DV, whereas CUT3R and TTT3R are trained on DL3DV and RealEstate10K but not ACID. In contrast, StreamVGGT and WinT3R are not trained on any of the three evaluation datasets. ReCoSplat consistently outperforms all autoregressive baselines across the three benchmarks. In particular, on RealEstate10K, we achieve substantially higher accuracy than CUT3R and TTT3R despite these methods being trained on that dataset. On ACID, which is unseen during training for all models, our method also achieves the strongest performance among autoregressive ap-

**Table 4:** Camera pose estimation results on ACID, RealEstate10K, and DL3DV. We report the AUC of the angular pose error curve at  $5^\circ$ ,  $10^\circ$ , and  $20^\circ$  thresholds for different numbers of input views. The **best** and **second best** metrics are marked, excluding offline methods.

| Method     | Online | ACID               |                              |                     |                    |                              |                     | RealEstate10K      |                              |                     |                    |                               |                     | DL3DV              |                               |                     |                    |                               |                     |
|------------|--------|--------------------|------------------------------|---------------------|--------------------|------------------------------|---------------------|--------------------|------------------------------|---------------------|--------------------|-------------------------------|---------------------|--------------------|-------------------------------|---------------------|--------------------|-------------------------------|---------------------|
|            |        | $5^\circ \uparrow$ | $32v$<br>$10^\circ \uparrow$ | $20^\circ \uparrow$ | $5^\circ \uparrow$ | $64v$<br>$10^\circ \uparrow$ | $20^\circ \uparrow$ | $5^\circ \uparrow$ | $64v$<br>$10^\circ \uparrow$ | $20^\circ \uparrow$ | $5^\circ \uparrow$ | $128v$<br>$10^\circ \uparrow$ | $20^\circ \uparrow$ | $5^\circ \uparrow$ | $128v$<br>$10^\circ \uparrow$ | $20^\circ \uparrow$ | $5^\circ \uparrow$ | $256v$<br>$10^\circ \uparrow$ | $20^\circ \uparrow$ |
| YoNoSplat  | X      | 0.493              | 0.670                        | 0.787               | 0.475              | 0.661                        | 0.783               | 0.701              | 0.846                        | 0.921               | 0.685              | 0.834                         | 0.911               | 0.741              | 0.870                         | 0.935               | 0.738              | 0.869                         | 0.935               |
| CUT3R      |        | 0.163              | 0.379                        | 0.587               | 0.105              | 0.312                        | 0.528               | 0.282              | 0.547                        | 0.754               | 0.140              | 0.411                         | 0.666               | 0.106              | 0.398                         | 0.670               | 0.065              | 0.024                         | 0.244               |
| TTFR       |        | 0.193              | 0.409                        | 0.611               | 0.159              | 0.376                        | 0.588               | 0.301              | 0.776                        | 0.270               | 0.539              | 0.748                         | 0.324               | 0.754              | 0.877                         | 0.263               | 0.570              | 0.785                         |                     |
| StreamVGGT |        | 0.028              | 0.153                        | 0.382               | 0.018              | 0.124                        | 0.348               | 0.021              | 0.164                        | 0.428               | 0.014              | 0.133                         | 0.393               | 0.012              | 0.146                         | 0.427               | OOM                | OOM                           | OOM                 |
| WinTR      |        | 0.042              | 0.177                        | 0.381               | 0.016              | 0.094                        | 0.252               | 0.186              | 0.465                        | 0.700               | 0.077              | 0.294                         | 0.562               | 0.100              | 0.372                         | 0.648               | 0.011              | 0.117                         | 0.389               |
| Ours       |        | 0.444              | 0.635                        | 0.764               | 0.406              | 0.607                        | 0.749               | 0.689              | 0.839                        | 0.917               | 0.666              | 0.823                         | 0.905               | 0.715              | 0.857                         | 0.928               | 0.709              | 0.854                         | 0.927               |

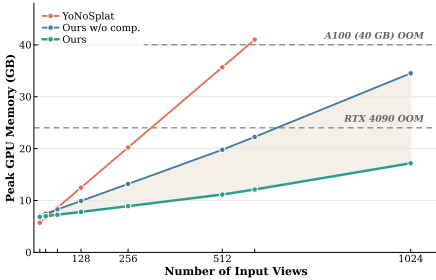


**Fig. 5:** Peak GPU memory usage on an A6000 GPU. KV-cache compression significantly suppresses memory usage compared to YoNoSplat and an uncompressed baseline. OOM thresholds for common GPU models are marked.



**Fig. 6:** Novel view synthesis on ScanNet (out-of-distribution) with 32 input views in the posed and calibrated setting.

proaches, demonstrating strong generalization to new scene distributions. While the offline baseline YoNoSplat achieves higher pose accuracy, it benefits from access to the entire image set during inference. In contrast, ReCoSplat estimates camera poses autoregressively from streaming observations while maintaining competitive accuracy across all datasets.

### 4.3 Ablation Study

We perform ablations to analyze key design choices in ReCoSplat. Table 5 studies pose supervision and conditioning strategies using models trained with up to 32 input views to reduce training time. Table 6 evaluates chunk-size curriculum learning and KV cache compression using 128 input views. These experiments use Stage 2 or Stage 3 checkpoints, which allow for evaluation on larger view counts. All experiments are conducted on DL3DV.

**Predicted Assembly Pose.** In Section 3.3, we noted that training with predicted assembly poses couples local Gaussian prediction with camera pose estimation, which can destabilize training. To evaluate this effect, we train a model

**Table 5:** We compare training with predicted, ground-truth, and mixed assembly poses, as well as Plücker raymap conditioning, using a KV-cache backbone on DL3DV with 32 input views.

| Method                             | Stage $p$ | $k$ | PSNR $\uparrow$ | SSIM $\uparrow$ | LPIPS $\downarrow$ |
|------------------------------------|-----------|-----|-----------------|-----------------|--------------------|
| KV Cache                           | 1         | ✓   | 21.346          | 0.680           | 0.224              |
| KV Cache + Predicted Assembly Pose | 1         | ✓   | 20.781          | 0.641           | 0.238              |
| KV Cache + Mixed Assembly Pose     | 1         | ✓   | 21.316          | 0.681           | 0.223              |
| KV Cache + Plücker Raymap          | 1         | ✓   | 21.166          | 0.676           | 0.228              |
| KV Cache                           | 1         | ✓   | 21.866          | 0.729           | 0.196              |
| KV Cache + Predicted Assembly Pose | 1         | ✓   | 20.836          | 0.656           | 0.229              |
| KV Cache + Mixed Assembly Pose     | 1         | ✓   | 21.915          | 0.736           | 0.192              |
| KV Cache + Plücker Raymap          | 1         | ✓   | 22.067          | 0.744           | 0.189              |

**Table 6:** We evaluate the effect of chunk-size curriculum learning (CL) and KV cache compression on DL3DV with 128 input views.

| Method                                  | Stage $p$ | $k$ | PSNR $\uparrow$ | SSIM $\uparrow$ | LPIPS $\downarrow$ |
|---|-----------|-----|-----------------|-----------------|--------------------|
| Ours                                    | 2         | ✓   | 21.527          | 0.689           | 0.227              |
| Ours w/o CL                             | 2         | ✓   | 21.510          | 0.688           | 0.227              |
| Ours @ Chunk Size (8, 4, 4, ...)        | 2         | ✓   | 21.397          | 0.680           | 0.237              |
| Ours w/o CL @ Chunk size (8, 4, 4, ...) | 2         | ✓   | 20.777          | 0.652           | 0.265              |
| Ours                                    | 3         | ✓   | 21.576          | 0.690           | 0.227              |
| Ours                                    | 2         | ✓   | 22.908          | 0.780           | 0.174              |
| Ours w/o CL                             | 2         | ✓   | 22.884          | 0.779           | 0.175              |
| Ours @ Chunk Size (8, 4, 4, ...)        | 2         | ✓   | 22.816          | 0.775           | 0.181              |
| Ours w/o CL @ Chunk Size (8, 4, 4, ...) | 2         | ✓   | 21.853          | 0.740           | 0.215              |
| Ours                                    | 3         | ✓   | 22.852          | 0.777           | 0.176              |

using predicted assembly poses. As shown in Table 5, this significantly degrades reconstruction quality compared to the KV cache baseline.

**Mixed Assembly Pose.** We also evaluate training with mixed ground-truth and predicted assembly poses. Table 5 shows negligible differences compared to using ground-truth poses alone, indicating that predicted poses provide limited supervision in the autoregressive setting.

**Plücker Raymap.** We test Plücker raymap conditioning to isolate the value of appearance-based conditioning. Plücker raymaps encode camera rays but do not incorporate information about the current reconstruction. Table 5 shows that this approach performs worse than the baseline when predicted poses are used at inference, indicating that geometric ray information alone is insufficient to correct pose-induced reconstruction errors.

**KV Cache Compression.** Table 6 shows that KV cache compression has minimal impact on reconstruction quality, while Figure 5 demonstrates substantial VRAM reductions at high view counts.

**Chunk-Size Curriculum Learning (CL).** The chunk-size training curriculum enables inference with variable chunk sizes with minimal performance variance (Table 6). We also observe no degradation in performance compared to training with a fixed chunk size ( $n = 8$ ).

## 5 Conclusion

In this work, we present ReCoSplat, an autoregressive feed-forward Gaussian Splatting framework for online novel view synthesis from sequential observations. We introduce a Render-and-Compare module to bridge the pose distribution mismatch between ground-truth and predicted assembly poses, enabling robust reconstruction in posed and unposed settings. To support long sequences, we further propose a KV cache compression strategy that greatly reduces memory usage while maintaining reconstruction quality. Experiments across multiple datasets and input configurations show that ReCoSplat achieves state-of-the-art performance among autoregressive approaches while remaining competitive with offline methods.

**Limitations.** While ReCoSplat improves robustness to pose errors by bridging the distribution mismatch between ground-truth and predicted assembly poses, reconstruction quality in unposed settings cannot be fully independent of pose estimation accuracy. Large pose errors can still propagate to Gaussian assembly and affect rendering fidelity. Advances in online pose estimation are therefore likely to further strengthen autoregressive reconstruction performance.

**Acknowledgements.** We thank Sifei Liu for extensive discussions and insightful suggestions that helped improve this work. We also thank Shuo Chen and Kuan-Chih Huang for helpful discussions.

## References

1. Charatan, D., Li, S., Tagliasacchi, A., Sitzmann, V.: pixelsplat: 3d gaussian splats from image pairs for scalable generalizable 3d reconstruction. In: CVPR (2024)
2. Chen, S., Wei, C., Sun, S., Nie, P., Zhou, K., Zhang, G., Yang, M.H., Chen, W.: Context forcing: Consistent autoregressive video generation with long context. arXiv preprint arXiv:2602.06028 (2026)
3. Chen, X., Chen, Y., Xiu, Y., Geiger, A., Chen, A.: Ttt3r: 3d reconstruction as test-time training. arXiv preprint arXiv:2509.26645 (2025)
4. Cheng, C., Yu, S., Wang, Z., Zhou, Y., Wang, H.: Outdoor monocular slam with global scale-consistent 3d gaussian pointmaps. In: Proceedings of the IEEE/CVF International Conference on Computer Vision (ICCV) (2025)
5. Dai, A., Chang, A.X., Savva, M., Halber, M., Funkhouser, T., Nießner, M.: Scannet: Richly-annotated 3d reconstructions of indoor scenes. In: Proc. Computer Vision and Pattern Recognition (CVPR), IEEE (2017)
6. Dosovitskiy, A., Beyer, L., Kolesnikov, A., Weissenborn, D., Zhai, X., Unterthiner, T., Dehghani, M., Minderer, M., Heigold, G., Gelly, S., Uszkoreit, J., Houlsby, N.: An image is worth 16x16 words: Transformers for image recognition at scale. In: International Conference on Learning Representations (2021)
7. Edstedt, J., Sun, Q., Bökman, G., Wadenbäck, M., Felsberg, M.: RoMa: Robust Dense Feature Matching. In: IEEE Conference on Computer Vision and Pattern Recognition (2024)
8. Guo, J., Guan, T., Dong, W., Zheng, W., Wang, W., Wang, Y., Yam, Y., Liu, Y.H.: Salon3r: Structure-aware long-term generalizable 3d reconstruction from unposed images. arXiv preprint arXiv:2510.15072 (2025)
9. Huang, G., Wang, R., Gao, X., Sun, C., Wu, Y., Gao, S., Jia, Y.: Longsplat: Online generalizable 3d gaussian splatting from long sequence images. arXiv preprint arXiv:2507.16144 (2025)
10. Jiang, L., Mao, Y., Xu, L., Lu, T., Ren, K., Jin, Y., Xu, X., Yu, M., Pang, J., Zhao, F., et al.: Anysplat: Feed-forward 3d gaussian splatting from unconstrained views. ACM Transactions on Graphics (TOG) **44**(6), 1–16 (2025)
11. Keetha, N., Müller, N., Schönberger, J., Porzi, L., Zhang, Y., Fischer, T., Knapitsch, A., Zauss, D., Weber, E., Antunes, N., Luiten, J., Lopez-Antequera, M., Bulò, S.R., Richardt, C., Ramanan, D., Scherer, S., Kotschieder, P.: MapAnything: Universal feed-forward metric 3D reconstruction. In: International Conference on 3D Vision (3DV). IEEE (2026)
12. Kerbl, B., Kopanas, G., Leimkühler, T., Drettakis, G.: 3d gaussian splatting for real-time radiance field rendering. ACM Transactions on Graphics **42**(4) (July 2023)

13. Li, Y., Wang, J., Chu, L., Li, X., Kao, S.H., Chen, Y.C., Lu, Y.: Streamsg: Online generalizable gaussian splatting reconstruction for unposed image streams. In: Proceedings of the IEEE/CVF International Conference on Computer Vision (ICCV). pp. 25841–25850 (October 2025)
14. Li, Z., Zhou, J., Wang, Y., Guo, H., Chang, W., Zhou, Y., Zhu, H., Chen, J., Shen, C., He, T.: Wint3r: Window-based streaming reconstruction with camera token pool. arXiv preprint arXiv:2509.05296 (2025)
15. Lin, H., Chen, S., Liew, J.H., Chen, D.Y., Li, Z., Shi, G., Feng, J., Kang, B.: Depth anything 3: recovering the visual space from any views. arXiv preprint arXiv:2511.10647 (2025)
16. Ling, L., Sheng, Y., Tu, Z., Zhao, W., Xin, C., Wan, K., Yu, L., Guo, Q., Yu, Z., Lu, Y., et al.: D13dv-10k: A large-scale scene dataset for deep learning-based 3d vision. In: Proceedings of the IEEE/CVF Conference on Computer Vision and Pattern Recognition. pp. 22160–22169 (2024)
17. Liu, A., Tucker, R., Jampani, V., Makadia, A., Snavely, N., Kanazawa, A.: Infinite nature: Perpetual view generation of natural scenes from a single image. In: Proceedings of the IEEE/CVF International Conference on Computer Vision (ICCV) (October 2021)
18. Oquab, M., Darcet, T., Moutakanni, T., Vo, H.V., Szafraniec, M., Khalidov, V., Fernandez, P., HAZIZA, D., Massa, F., El-Nouby, A., Assran, M., Ballas, N., Galuba, W., Howes, R., Huang, P.Y., Li, S.W., Misra, I., Rabbat, M., Sharma, V., Synnaeve, G., Xu, H., Jegou, H., Mairal, J., Labatut, P., Joulin, A., Bojanowski, P.: DINOv2: Learning robust visual features without supervision. Transactions on Machine Learning Research (2024), featured Certification
19. Ranftl, R., Bochkovskiy, A., Koltun, V.: Vision transformers for dense prediction. In: Proceedings of the IEEE/CVF International Conference on Computer Vision (ICCV). pp. 12179–12188 (October 2021)
20. Sarlin, P.E., DeTone, D., Malisiewicz, T., Rabinovich, A.: SuperGlue: Learning feature matching with graph neural networks. In: CVPR (2020)
21. Sun, X., Zhu, Z., Lou, Z., Yang, B., Tang, J., Zhang, L., Wang, H., Zhang, J.: Avggt: Rethinking global attention for accelerating vgg. arXiv preprint arXiv:2512.02541 (2025)
22. Sun, Y., Li, X., Dalal, K., Xu, J., Vikram, A., Zhang, G., Dubois, Y., Chen, X., Wang, X., Koyejo, S., Hashimoto, T., Guestrin, C.: Learning to (learn at test time): Rnns with expressive hidden states (2025)
23. Szymanowicz, S., Rupprecht, C., Vedaldi, A.: Splatter image: Ultra-fast single-view 3d reconstruction. In: The IEEE/CVF Conference on Computer Vision and Pattern Recognition (CVPR) (2024)
24. Wang, J., Chen, M., Karaev, N., Vedaldi, A., Rupprecht, C., Novotny, D.: Vggt: Visual geometry grounded transformer. In: Proceedings of the IEEE/CVF Conference on Computer Vision and Pattern Recognition (2025)
25. Wang\*, Q., Zhang\*, Y., Holynski, A., Efros, A.A., Kanazawa, A.: Continuous 3d perception model with persistent state. In: CVPR (2025)
26. Wang, S., Leroy, V., Cabon, Y., Chidlovskii, B., Revaud, J.: Dust3r: Geometric 3d vision made easy. In: Proceedings of the IEEE/CVF Conference on Computer Vision and Pattern Recognition (CVPR). pp. 20697–20709 (June 2024)
27. Wang, Y., Zhou, J., Zhu, H., Chang, W., Zhou, Y., Li, Z., Chen, J., Pang, J., Shen, C., He, T.:  $\pi^3$ : Permutation-equivariant visual geometry learning. arXiv preprint arXiv:2507.13347 (2025)

28. Wang, Y., Huang, T., Chen, H., Lee, G.H.: Freesplat: Generalizable 3d gaussian splatting towards free view synthesis of indoor scenes. In: The Thirty-eighth Annual Conference on Neural Information Processing Systems (2024)
29. Wang, Y., Huang, T., Chen, H., Lee, G.H.: Freesplat: Generalizable 3d gaussian splatting towards free view synthesis of indoor scenes. In: Globerson, A., Mackey, L., Belgrave, D., Fan, A., Paquet, U., Tomczak, J., Zhang, C. (eds.) *Advances in Neural Information Processing Systems*. vol. 37, pp. 107326–107349. Curran Associates, Inc. (2024)
30. Wu, T., Yang, S., Po, R., Xu, Y., Liu, Z., Lin, D., Wetzstein, G.: Video world models with long-term spatial memory. In: The Thirty-ninth Annual Conference on Neural Information Processing Systems (2025)
31. Wu, Y., Zheng, W., Zhou, J., Lu, J.: Point3r: Streaming 3d reconstruction with explicit spatial pointer memory. In: The Thirty-ninth Annual Conference on Neural Information Processing Systems (2025)
32. Xu, H., Peng, S., Wang, F., Blum, H., Barath, D., Geiger, A., Pollefeys, M.: Depth-splat: Connecting gaussian splatting and depth. In: CVPR (2025)
33. Yao, Y., Luo, Z., Li, S., Fang, T., Quan, L.: Mvsnet: Depth inference for unstructured multi-view stereo. *European Conference on Computer Vision (ECCV)* (2018)
34. Yao, Y., Luo, Z., Li, S., Shen, T., Fang, T., Quan, L.: Recurrent mvsnet for high-resolution multi-view stereo depth inference. *Computer Vision and Pattern Recognition (CVPR)* (2019)
35. Ye, B., Chen, B., Xu, H., Barath, D., Pollefeys, M.: Yonosplat: You only need one model for feedforward 3d gaussian splatting. In: *International Conference on Learning Representations (ICLR)* (2026)
36. Ye, B., Liu, S., Xu, H., Li, X., Pollefeys, M., Yang, M.H., Peng, S.: No pose, no problem: Surprisingly simple 3d gaussian splats from sparse unposed images. In: *The Thirteenth International Conference on Learning Representations* (2025)
37. Yeshwanth, C., Liu, Y.C., Nießner, M., Dai, A.: Scannet++: A high-fidelity dataset of 3d indoor scenes. In: *Proceedings of the International Conference on Computer Vision (ICCV)* (2023)
38. Yuille, A., Kersten, D.: Vision as bayesian inference: analysis by synthesis? *Trends in Cognitive Sciences* **10**(7), 301–308 (2006), special issue: Probabilistic models of cognition
39. Zhang, J., Li, Y., Chen, A., Xu, M., Liu, K., Wang, J., Long, X.X., Liang, H., Xu, Z., Su, H., Theobalt, C., Rupperecht, C., Vedaldi, A., Zhou, K., Pfister, H., Liang, P.P., Lu, S., Zhan, F.: Advances in feed-forward 3d reconstruction and view synthesis: A survey (2025)
40. Zhang, K., Bi, S., Tan, H., Xiangli, Y., Zhao, N., Sunkavalli, K., Xu, Z.: Gs-irm: Large reconstruction model for 3d gaussian splatting. *European Conference on Computer Vision* (2024)
41. Zhang, R., Isola, P., Efros, A.A., Shechtman, E., Wang, O.: The unreasonable effectiveness of deep features as a perceptual metric. In: CVPR (2018)
42. Zhou, T., Tucker, R., Flynn, J., Fyffe, G., Snavely, N.: Stereo magnification: Learning view synthesis using multiplane images. In: SIGGRAPH (2018)
43. Zhuo, D., Zheng, W., Guo, J., Wu, Y., Zhou, J., Lu, J.: Streaming 4d visual geometry transformer. *arXiv preprint arXiv:2507.11539* (2025)

## A Appendix

### A.1 Video Results

Video results can be found at our project page: <https://freemancheng.com/ReCoSplat>.

### A.2 Additional Ablation Studies

**Gaussian Features.** To enrich the conditioning signal within the Render-and-Compare module, we augment each Gaussian with nine learned feature dimensions alongside standard RGB. These features are rendered with the RGB channels, providing auxiliary cues regarding the current scene reconstruction to better align the rendered and observed images. Table 7 evaluates the impact of removing these features on the DL3DV [16] dataset. Without them, ReCoSplat exhibits a noticeable drop in performance during inference when utilizing predicted assembly poses. This drop indicates that these auxiliary feature channels supply critical contextual information for mitigating pose-induced reconstruction errors. To minimize training overhead, all models evaluated in Table 7 were trained using a maximum of 32 context views. For completeness, we also include the corresponding results from Table 5 of the main text. Finally, Figure 7 provides a PCA-projected visualization of these rendered Gaussian feature maps.

**Table 7:** Ablation study on DL3DV (32 input views) evaluating the impact of augmenting Gaussians with additional feature dimensions for the Render-and-Compare module. Removing these features degrades reconstruction quality when predicted assembly poses are used at inference, indicating that the learned feature channels provide essential context for correcting pose-induced errors. **Best** and **second-best** results are highlighted.

| Method                             | Stage $p$ | $k$ | PSNR $\uparrow$ | SSIM $\uparrow$ | LPIPS $\downarrow$ |
|------------------------------------|-----------|-----|-----------------|-----------------|--------------------|
| KV Cache                           | 1         | ✓   | 21.346          | 0.680           | 0.224              |
| KV Cache + Predicted Assembly Pose | 1         | ✓   | 20.781          | 0.641           | 0.238              |
| KV Cache + Mixed Assembly Pose     | 1         | ✓   | 21.316          | 0.681           | 0.223              |
| KV Cache + Plücker Raymap          | 1         | ✓   | 21.166          | 0.676           | 0.228              |
| Ours w/o Gaussian Features         | 1         | ✓   | 21.455          | 0.685           | 0.223              |
| Ours                               | 1         | ✓   | <b>21.769</b>   | <b>0.699</b>    | <b>0.212</b>       |
| KV Cache                           | 1         | ✓✓  | 21.866          | 0.729           | 0.196              |
| KV Cache + Predicted Assembly Pose | 1         | ✓✓  | 20.836          | 0.656           | 0.229              |
| KV Cache + Mixed Assembly Pose     | 1         | ✓✓  | 21.915          | 0.736           | 0.192              |
| KV Cache + Plücker Raymap          | 1         | ✓✓  | 22.067          | 0.744           | 0.189              |
| Ours w/o Gaussian Features         | 1         | ✓✓  | 22.548          | <b>0.759</b>    | 0.181              |
| Ours                               | 1         | ✓✓  | <b>22.610</b>   | <b>0.759</b>    | <b>0.178</b>       |



**Fig. 7:** Visualization of the additional Gaussian feature channels rendered by our model, reduced to three dimensions via PCA projection.

**Prompt Register Token.** As shown in Table 8, introducing the prompt register token yields negligible performance differences on the DL3DV dataset. In contrast, it provides consistent performance gains on ScanNet++ [37] (Table 9), a dataset characterized by irregular camera trajectories for the streaming setting. This contrast highlights that explicitly marking retained views in the KV cache is particularly beneficial for when camera motion irregular for the streaming setting.

**Table 8:** Ablation study evaluating the prompt register token on the DL3DV dataset across varying numbers of input views. Explicitly marking retained views yields minimal performance changes on these smoother sequences. **Best** results are highlighted.

| Method                | $p$ | $k$ | 90v             |                 |                    | 180v            |                 |                    | 270v            |                 |                    |
|-----------------------|-----|-----|-----------------|-----------------|--------------------|-----------------|-----------------|--------------------|-----------------|-----------------|--------------------|
|                       |     |     | PSNR $\uparrow$ | SSIM $\uparrow$ | LPIPS $\downarrow$ | PSNR $\uparrow$ | SSIM $\uparrow$ | LPIPS $\downarrow$ | PSNR $\uparrow$ | SSIM $\uparrow$ | LPIPS $\downarrow$ |
| Ours w/o Prompt Token | ✓   |     | 21.175          | 0.669           | 0.238              | 20.820          | 0.649           | 0.261              | <b>20.365</b>   | <b>0.626</b>    | 0.284              |
| Ours                  | ✓   |     | <b>21.206</b>   | <b>0.670</b>    | <b>0.237</b>       | <b>20.823</b>   | <b>0.651</b>    | <b>0.259</b>       | 20.325          | 0.625           | <b>0.282</b>       |

**Table 9:** Ablation study evaluating the prompt register token on the ScanNet++ dataset. The inclusion of the prompt token yields consistent improvements due to ScanNet++’s highly irregular camera trajectories, which benefit significantly from explicitly marking retained views in the KV cache. **Best** results are highlighted.

| Method                | $p$ | $k$ | 128v            |                 |                    | 256v            |                 |                    | 512v            |                 |                    |
|-----------------------|-----|-----|-----------------|-----------------|--------------------|-----------------|-----------------|--------------------|-----------------|-----------------|--------------------|
|                       |     |     | PSNR $\uparrow$ | SSIM $\uparrow$ | LPIPS $\downarrow$ | PSNR $\uparrow$ | SSIM $\uparrow$ | LPIPS $\downarrow$ | PSNR $\uparrow$ | SSIM $\uparrow$ | LPIPS $\downarrow$ |
| Ours w/o Prompt Token | ✓   |     | 19.635          | 0.675           | 0.337              | 19.492          | 0.654           | 0.351              | 17.791          | 0.594           | 0.438              |
| Ours                  | ✓   |     | <b>19.840</b>   | <b>0.683</b>    | <b>0.331</b>       | <b>19.660</b>   | <b>0.663</b>    | <b>0.342</b>       | <b>18.289</b>   | <b>0.611</b>    | <b>0.411</b>       |

### A.3 Additional Visual Comparisons

We provide extended visual comparisons in Figures 8 and 9. Figure 8 illustrates novel view synthesis results on ScanNet [5] in the fully posed setting using 32 input views. ReCoSplat visibly outperforms both autoregressive baselines and FreeSplat [29], demonstrating robust generalization even on out-of-distribution

data. These visual improvements align closely with the quantitative results presented in Tables 2. Furthermore, as noted in Section 4.2, our method surpasses the offline baseline YoNoSplat [35] in PSNR under fully posed conditions. Specific examples of this can be seen in the third and fourth rows of Figure 8. Finally, Figure 9 demonstrates comparative novel view synthesis on DL3DV across various unposed input settings, providing further qualitative evidence of ReCoSplat’s advantage over the autoregressive baselines.

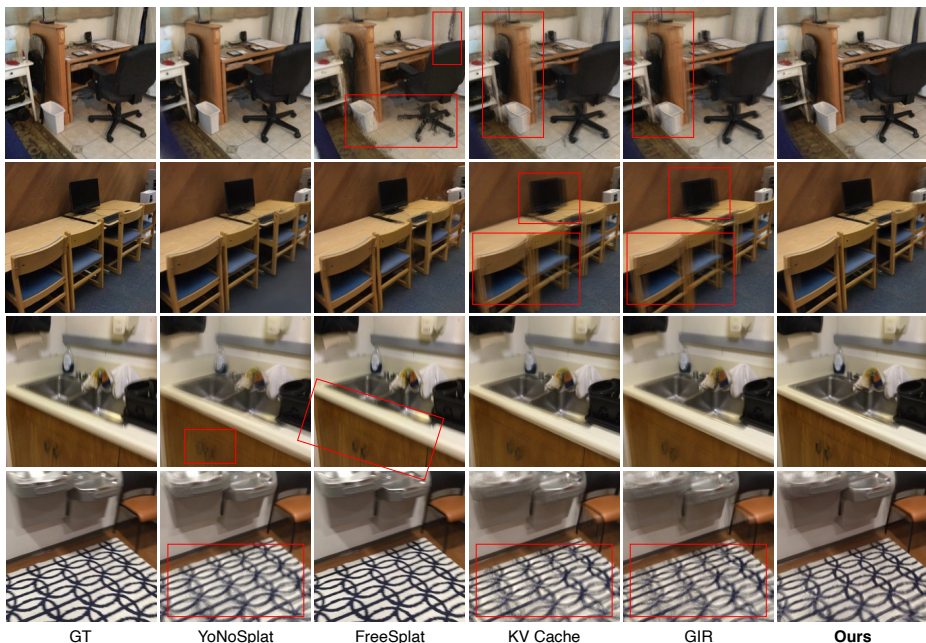


**Fig. 8:** Novel view synthesis on ScanNet (out-of-distribution) with 32 input views in the posed and calibrated setting.

#### A.4 Loss Formulation

**Relative Pose Loss.**  $\mathcal{L}_{\text{extrinsic}}$  is a pairwise relative pose loss [35]. For any pair of views  $i$  and  $j$  indexed on the entire input sequence of length  $N$ , let  $P_i = [R_i, t_i]$  and  $P_j = [R_j, t_j]$  represent their respective ground-truth poses, while  $\hat{P}_i = [\hat{R}_i, \hat{t}_i]$  and  $\hat{P}_j = [\hat{R}_j, \hat{t}_j]$  denote the model’s predictions. Following [35]’s notation, we denote the relative transformation from the  $j$ -th predicted pose to the  $i$ -th predicted pose as  $\hat{P}_{i \leftarrow j} = \hat{P}_i^{-1} \hat{P}_j$ , and similarly for the ground truth,  $P_{i \leftarrow j} = P_i^{-1} P_j$ . Then, our loss is decomposed into rotation and translation

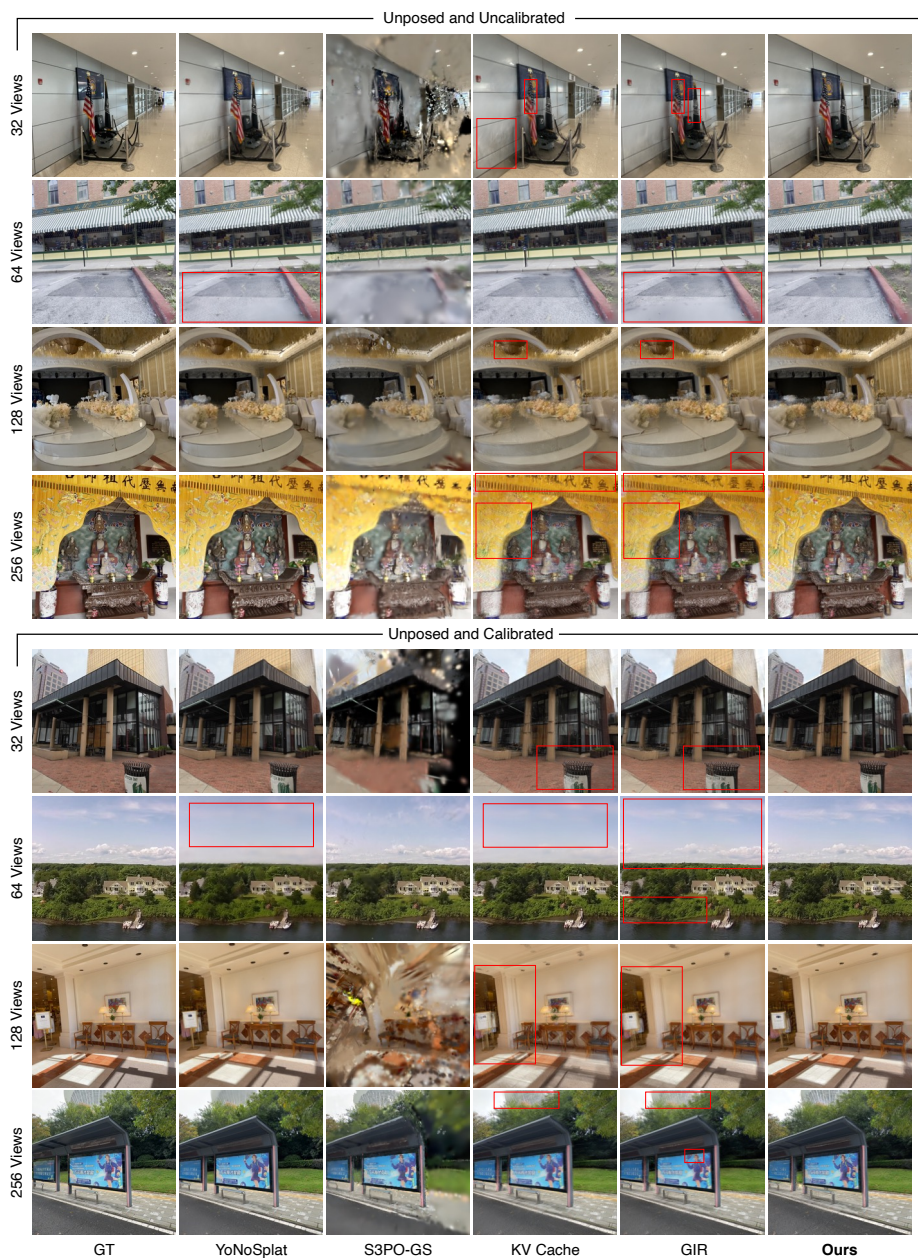


**Fig. 9:** Novel view synthesis on DL3DV with an increasing number of input views under unposed settings. Note that while S3PO-GS typically requires calibrated inputs, we include it here for comparison in the uncalibrated setting.

terms

$$\mathcal{L}_{\text{extrinsic}} = \frac{1}{N(N-1)} \sum_{i \neq j} (\mathcal{L}_R(i, j) + \lambda_t \mathcal{L}_t(i, j)) \quad (10)$$

where

$$\mathcal{L}_R(i, j) = \arccos \left( \frac{\text{tr} \left( (R_{i \leftarrow j})^\top \hat{R}_{i \leftarrow j} \right) - 1 \right)}{2} \right) \quad (11)$$

and

$$\mathcal{L}_t(i, j) = \mathcal{H}_\delta (\hat{t}_{i \leftarrow j} - t_{i \leftarrow j}). \quad (12)$$

Here,  $\mathcal{H}_\delta$  is the Huber loss.